

Testing the Blazar Paradigm: *ASCA* Observations of FSRQs with Steep Soft X-ray Spectra

Rita M. Sambruna and Lester L. Chou

The Pennsylvania State University, Department of Astronomy and Astrophysics, 525
Davey Lab, State College, PA 16802

C. Megan Urry

STScI, 3700 San Martin Dr., Baltimore, MD 21218

ABSTRACT

We present the first observations at medium-hard X-rays with *ASCA* in 1998 August–November of four Flat Spectrum Radio Quasars (FSRQs), characterized by unusually steep soft X-ray spectra (photon index, $\Gamma_{0.2-2.4 \text{ keV}} \sim 2 - 2.5$), as previously measured with *ROSAT*. Such steep X-ray slopes are similar to those observed in synchrotron-dominated BL Lacs and are unexpected in the context of the recent blazar paradigm, where sources with strong emission lines (such as FSRQs) are dominated in soft X-rays by a flat inverse Compton tail. We find that the *ASCA* spectra of the four FSRQs are consistent with a power law model with $\Gamma_{2-10 \text{ keV}} \sim 1.8$, flatter than their *ROSAT* spectra. This indicates the onset of an inverse Compton component at energies $\gtrsim 2 \text{ keV}$, in agreement with the blazar unification scheme. However, these objects are still anomalous within the blazar class for their steep soft X-ray continua which, together with non-simultaneous data at longer wavelengths, hint at the possibility that the synchrotron emission extends to soft X-rays. This would imply an anomalously high synchrotron peak frequency for a quasar with luminous broad lines, challenging current blazar unification schemes. Alternatively, a plausible explanation for the steep optical-to-soft X-ray continua of the four FSRQs is thermal emission from the accretion disk, similar to the blazars 3C 273 and 3C 345. In the Appendix, we present fits to the SIS data in an effort to contribute to the ongoing calibration of the the time-dependence of the SIS response at low energies.

1. Introduction

Among radio-loud AGN, the subclass of blazars stands out for its large luminosities and rapid variability timescales observed from radio to γ -rays (Ulrich, Maraschi, & Urry

1997; von Montigny et al. 1995; Angel & Stockman 1980). This can be readily explained as non-thermal emission from a relativistic jet oriented at close angles to the line of sight (Urry & Padovani 1995; Blandford & Rees 1978). While these continuum properties encompass the entire blazar class, a further traditional subdivision is based on the strength of the optical emission lines, with BL Lacertae objects (BL Lacs) having weaker lines than Flat Spectrum Radio Quasars (FSRQs). However, since the distribution of the line luminosity is continuous across the blazar class (Scarpa & Falomo 1997; Padovani 1992), the division between BL Lacs and FSRQs is not bimodal but based on an arbitrary equivalent width criterion.

More than twenty years after their discovery in the late 1970s, the blazar “zoo” has been ordered according to the shape of the observed spectral energy distributions (SEDs) from radio to γ -rays. The SEDs appear to have a universal shape, with two distinct components (Fossati et al. 1997; Sambruna, Maraschi, & Urry 1996; Giommi, Ansari, & Micol 1995). The first component peaks anywhere from radio to UV/X-rays and is interpreted as synchrotron emission from the jet because it is highly variable, especially at higher energies, and polarized (Ulrich et al. 1997). The second component extends to γ -rays and its origin can be interpreted as inverse Compton scattering of ambient photons off the jet electrons, either internal (synchrotron-self Compton, SSC; Maraschi, Ghisellini, & Celotti 1992) or external (external Compton, EC; Ghisellini & Madau 1996; Sikora, Begelman, & Rees 1994; Dermer, Schlickseier, & Mastichiadis 1992), although there are alternative scenarios, such as the hadronic models (Protheroe & Biermann 1997; Mannheim & Biermann 1992). Depending on the position of the synchrotron peak, blazars are classified as High-energy peaked, or HBLs (peak in UV/X-rays) or Low-energy peaked, or LBLs (peak in IR/optical). An equivalent empirical division is given by the ratio of the radio to X-ray fluxes, with $\alpha_{rx} \lesssim 0.8$ in HBLs and $\alpha_{rx} \gtrsim 0.8$ in LBLs (Padovani & Giommi 1995). FSRQs have SEDs similar to LBLs and higher bolometric luminosities (Padovani, Giommi, & Fiore 1997; Sambruna 1997).

With the advent of deeper multicolor spectral surveys (Laurent-Muehleisen et al. 1998; Perlman et al. 1998), it was quickly realized that the distribution of synchrotron peaks is continuous and not bimodal. FSRQs, LBLs, and HBLs can be arranged on a continuous spectral sequence characterized by decreasing bolometric and emission line luminosities, and increasing synchrotron frequency (Fossati et al. 1998, 1997; Sambruna 1997; Sambruna et al. 1996). In addition, the peak of the inverse Compton component appears to increase proportionally to the synchrotron one along the same sequence, while the ratio of the Compton to synchrotron luminosity decreases (Fossati et al. 1998). On the basis of these trends a new scheme was proposed where the transition from FSRQs to LBLs to HBLs is governed by a change of a few physical parameters (Sambruna et al. 1996; Fossati et

al. 1998) and/or a change in the jet gaseous environs (Ghisellini et al. 1998). However, selection biases especially at γ -rays need to be addressed before reaching firm conclusions (Urry 1999).

According to this tentative new paradigm, blazars with strong emission lines and/or thermal bumps (where the external radiation field is strong) should be EC dominated and thus always have flat continua at X-rays, where the inverse Compton tail dominates (Ghisellini et al. 1998). At the other extreme are HBLs, where, as a consequence of the high synchrotron peak frequencies, steep, convex (as a result of the synchrotron losses), and highly variable X-ray spectra should be observed. While recent observations with *ASCA* support this view (Sambruna et al. 1999; Kubo et al. 1998), studies of larger samples of FSRQs with *ROSAT* provided evidence for the existence of a sub-class of “X-ray-steep” FSRQs (Padovani, Giommi, & Fiore 1997; Sambruna 1997), with soft X-ray photon indices $\Gamma_{0.2-2.4 \text{ keV}} \gtrsim 2$, similar to HBLs. Moreover, recent multicolor blazar surveys revealed that a sizable fraction (40%) of the FSRQ population exhibit $\alpha_{rx} \lesssim 0.8$ (Perlman et al. 1998), similar to HBLs.

The existence of FSRQs with HBL-like spectra is unexpected in the context of the blazar paradigm and requires an explanation. To gain further insights we observed with *ASCA* four “X-ray-steep” FSRQs selected from our previous *ROSAT* study. The aim of our *ASCA* observations is to measure the medium-hard X-ray continuum: if synchrotron emission dominates the X-ray spectra of these systems, like in HBLs, their *ASCA* spectra will be steep or even curved, while if a Compton component is present (similar to most FSRQs) the *ASCA* spectra will be flatter than at softer energies. None of the four targets is a known γ -ray emitter, contrary to most of the FSRQs so far observed with *ASCA* (Kubo et al. 1998).

The structure of the paper is as follows. In § 2 we discuss the sample and the data, in § 3 the results of spectral fits, and in § 4 we briefly discuss the implications of our findings. Throughout the paper, $H_0=75 \text{ km s}^{-1} \text{ Mpc}^{-1}$ and $q_0 = 0.5$ are assumed.

2. *ASCA* Observations

2.1. The Sample

The targets of the present work are FSRQs with strong emission lines selected from our previous *ROSAT* study (Sambruna 1997) according to the following criteria: 1) they have steep X-ray spectra (photon index, $\Gamma_{0.2-2.4 \text{ keV}} \gtrsim 2$), as measured with the PSPC; 2) they are bright enough to obtain a high-quality *ASCA* spectrum in a reasonable exposure

time; and 3) they were never observed before at medium-hard X-rays. These criteria gave a list of 7 FSRQs, four of which were granted *ASCA* time during AO6.

The basic properties of the four FSRQs observed with *ASCA* are reported in Table 1, where we list their names (column 1), redshifts (column 2), the observed radio flux densities at 5 GHz and the *V* magnitudes (column 3), and the Galactic column densities N_H in the direction to the sources (column 4). The latter were obtained from the 21 cm maps of Elvis, Lockmann, & Wilkes (1989) and Stocke et al. (1992), and are accurate to $\pm 1 \times 10^{20} \text{ cm}^{-2}$ or better. The *ROSAT* slopes and 1 keV flux densities are summarized in columns 5 and 6, respectively, while columns 7–11 give the equivalent widths and luminosities of the optical lines (in the sources’ rest-frame), and the composite spectral indices between radio (5 GHz) and optical (*V* band), α_{ro} , between the optical and X-rays (1 keV), α_{ox} , and between radio and X-rays, α_{rx} . The emission lines’ parameters and the (non-simultaneous) multifrequency fluxes were taken from the literature. None of the sources in Table 1 was detected at γ -rays with EGRET (Hartman et al. 1999) or other currently operating detectors.

The composite spectral indices were evaluated using K-corrected flux densities. For the K-correction, the fluxes were multiplied by $(1+z)^{\alpha-1}$, where α is the energy index in the appropriate band ($F_\nu \propto \nu^{-\alpha}$). In the radio, individual slopes were used (Kühr et al. 1981 and Table 1). In the optical, we used $\langle \alpha_{opt} \rangle = 0.65$, the average slope for a sample of radio-selected blazars (Falomo, Scarpa, & Bersanelli 1994). In the X-rays, the individual slopes from the *ROSAT* PSPC observations were used (Table 1).

2.2. Data Reduction and Analysis

We observed the four sources during *ASCA* AO6 in late 1998. For a description of the *ASCA* experiment see Tanaka, Inoue, & Holt (1994). In all cases, the Solid-State Imaging Spectrometers (SIS0 and SIS1) operated in 1-CCD FAINT mode and the Gas Imaging Spectrometers (GIS2 and GIS3) were used in Pulse-Height mode. In order to apply standard data analysis methods, the FAINT SIS mode was converted into BRIGHT2, applying the corrections for echo effect and dark frame error (see “The *ASCA* Data Reduction Guide”, v.2, April 1997). Standard screening criteria were applied for the data reduction, including rejection of the data taken during the passage of the South Atlantic Anomaly and for geomagnetic cutoff rigidity lower than 6 GeV/c. We retained SIS data accumulated for Bright Earth angles $> 20^\circ$ and Elevation angles $> 10^\circ$, and GIS data accumulated for Elevation angles $> 5^\circ$. Only data corresponding to SIS grades 0, 2, 3, and 4 were accepted.

The source spectra and light curves were extracted from circular regions centered on

the source position with radii of 4 arcmin for the SIS and 6 arcmin for the GIS, which has a larger intrinsic point spread function. The background was evaluated from blank-sky observations in circular regions of the same size at the source’s position. We checked that larger extraction cells for the background and/or different positions on the chip do not affect the final results of our analysis. Details of the *ASCA* observations are reported in Table 2, which lists: the date of the observation (column 2), the net exposure after data screening (column 3), and the SIS0 and GIS2 net count rates in 0.6–10 keV and 0.7–10 keV, respectively.

Since no flux or spectral variability is apparent within the *ASCA* exposures, the spectra were integrated over the entire duration of the observations. The *ASCA* spectra were fitted using XSPEC v.10. The SIS and GIS spectra were rebinned in order to have a minimum of 20 counts in each spectral bin to validate the use of the χ^2 statistic. In order to increase the signal-to-noise ratio we performed joint fits to the data from the four detectors, leaving only the normalizations as independent parameters. The 1994 May response matrices were used for the GIS spectra, while for the SIS data we used the matrices generated by the SISRMG program (v.1.1, 1997 March). The SIS and GIS data were fitted in the energy ranges 0.6–10 keV and 0.7–10 keV, where the spectral responses are best known.

3. Spectral Fits and Results

We first fitted the *ASCA* data using a single power law model, modified at lower energies by the absorption column density N_H (in cm^{-2}). The Morrison & McCammon (1983) cross-section for photoelectric absorption was used, with the abundances of elements heavier than hydrogen fixed at solar values. In the spectral fits N_H was left both free and fixed to the Galactic value (from Table 1). It must be borne in mind that systematic effects are present in the two SIS detectors below 1–2 keV which lead to an overestimation of the column density (Dotani et al. 1996) by at least $3 \times 10^{20} \text{ cm}^{-2}$, which has been increasing with the aging of the mission (Yaqoob et al. 2000). Fits with free N_H must thus be taken with caution and are reported here for completeness only (see also Appendix). No excess absorption was detected in the previous *ROSAT* observations of the four blazars (Sambruna 1997).

The results from the fits to the *ASCA* data with a single power law model are reported in Table 3. The power law photon index, Γ , and the fitted N_H are reported together with their 90% confidence errors ($\Delta\chi^2=2.7$ for one parameter of interest) and the observed 2–10 keV flux, $F_{2-10 \text{ keV}}$. Figure 1 shows the residuals of the fit with a single power law plus fixed Galactic absorption to the *ASCA* data of the four targets (solid symbols). As apparent

from Table 3, the fits with fixed N_H are generally acceptable, although the fits with free N_H are improved, especially for 0923+392. The 0.6–10 keV spectra of the four FSRQs are characterized by relatively flat slopes, $\Gamma = 1.7 - 1.8$, similar to other FSRQs observed with *ASCA* (e.g., Kubo et al. 1998), and flatter than their *ROSAT* PSPC slopes (Table 1). This strongly suggests a different spectral component in the *ASCA* band, although spectral variability between the epochs of the *ROSAT* and *ASCA* observations can not be ruled out *a priori*. However, we note that little or no spectral variability is observed at both soft and hard X-rays for FSRQs repeatedly observed with *ROSAT* and *ASCA* (Sambruna 1997; Kubo et al. 1998). Moreover, our fits to the joint *ROSAT* and *ASCA* data (see below) are entirely consistent with the two detectors sampling distinct regions of the same continuum. We thus regard spectral variability as an unlikely explanation of the different *ROSAT* and *ASCA* slopes of our four FSRQs, and conclude that the broad-band X-ray spectra of the sources is complex, and a soft excess is present below ~ 1 keV.

In the assumption that the steeper *ROSAT* slopes belong to a different spectral component than *ASCA*, we attempted joint fits to the *ASCA* and (non-simultaneous) *ROSAT* data in order to characterize the shape of the soft excess. For 0405–123, 0923+392, and 1150+497, the *ROSAT* data lie above the extrapolation of the *ASCA* power law at energies $\lesssim 1$ keV (Figure 1, open symbols). We fitted the joint *ROSAT* and *ASCA* datasets of these three sources adding to the hard X-ray power law one of the following components to model the soft excess in the *ROSAT* band: a thermal bremsstrahlung, a blackbody, and a second steeper power law (double power law). During the fits, the column density was held fixed to the Galactic value for all datasets, except for SIS0 and SIS1, where it was left free to vary. The results of the fits with the three models are reported in Table 4. It is apparent that all models provide similar fits, and it is not possible to discriminate between a thermal and non-thermal origin of the soft excess. There is, however, a slight preference for the bremsstrahlung model for 0405–123 ($\Delta\chi^2 = 5$ over the double power law model), and for a non-thermal origin for 1150+497 (the double power law gives $\Delta\chi^2 = 10$ over the thermal models).

The last column of Table 4 lists the observed 0.2–10 keV and 0.2–2.0 keV fluxes determined from the best-fit model. The fraction of the total (0.2–10 keV) flux in the soft component, i.e., the ratio of the 0.2–2 keV flux to the total 0.2–10 keV flux, is 12% for 0405–123, 7% for 0923+392, and 12% for 1150+497.

In the case of 0736+017, the *ROSAT* plus *ASCA* data are well fitted by a single power law, with a slope close to that derived from the *ASCA* data only (Table 4). For this source, however, the *ROSAT* data have large error bars, especially below 0.5 keV where the absorption from the Galactic column density is large (Figure 1). We thus regard the

evidence for a soft excess in this source as tentative.

In summary, we measured with *ASCA* the medium-hard X-ray continua of four FSRQs characterized by steep 0.2–2.4 keV spectra and found them consistent with single power laws with photon indices $\Gamma \sim 1.8$. These are flatter than the *ROSAT* slopes and indicate a soft excess in at least three cases (0405–123, 0923+392, and 1150+497).

We are able to set interesting upper limits to the equivalent width (EW) of an Fe K α emission line at 6.4 keV in the four FSRQs. The Fe line is detected in other radio-loud AGN (Sambruna, Eracleous, & Mushotzky 1999) and in blazars like 3C 273 (Cappi et al. 1998; Grandi et al. 1997). In our targets the Fe line would be redshifted in the energy range 3–5 keV, close to the SIS sensitivity peak. We added a narrow (width=0.05 keV, or FWHM ~ 5600 km/s) Gaussian with rest-frame energy 6.4 keV to the power law plus Galactic absorption model and fitted the *ASCA* data. No fit improvement is obtained, with the 90% confidence upper limits on the Fe line EW of 47 eV for 0405–123 and 0923+392, 112 eV for 0736–017, and 81 eV for 1150+497. These are consistent with the upper limits found for lobe-dominated radio-loud quasars (Sambruna et al. 1999) and significantly lower than radio-quiet quasars of similar X-ray luminosity (Nandra et al. 1997).

4. Discussion and Conclusions

We have observed with *ASCA* four FSRQs characterized by unusually steep ($\Gamma_{0.2-2.4 \text{ keV}} \gtrsim 2$) X-ray spectra in the *ROSAT* band. Our principal result is that all four targets have flat continua at medium-hard X-rays described by photon indices $\Gamma_{2-10 \text{ keV}} \sim 1.8$. Formally, the average slope for the four targets is $\langle \Gamma_{2-10 \text{ keV}} \rangle = 1.81$ with 1σ dispersion 0.05 (from the fits with free N_H in Table 3). This is consistent with the average slope measured by *ASCA* for a group of 10 FSRQs, $\Gamma_{FSRQs} = 1.60$ with dispersion 0.14 (Sambruna et al. 1999). The latter group include mostly sources with strong γ -ray detections (Kubo et al. 1998), for which the flat X-ray continuum is interpreted as the onset of the inverse Compton component peaking at GeV energies, or high- z sources where the flat Compton tail is redshifted in the *ASCA* band. We thus conclude that our four targets are also dominated by the onset of the inverse Compton component at medium-hard X-rays.

The steep *ROSAT* spectra of the four targets, however, still imply unusual properties. To clarify this point we assembled (non-simultaneous) spectral energy distributions (SEDs) using our *ASCA* and *ROSAT* data and longer wavelength fluxes from the literature; the SEDs of the four sources are shown in Figure 2 (see caption for references). The radio, optical, and X-ray data were K-corrected following the procedure outlined in § 2.1. For

the IR data, we used $\langle\alpha_{IR}\rangle=1.27$, from observations of a sample of radio-selected blazars (Falomo et al. 1994). Although poorly sampled in the intermediate wavebands, the SEDs in Figure 2 suggest large emission in the optical/IR bands¹ which connects smoothly to the *ROSAT* flux in most cases. The SEDs have an upturn at medium-hard X-rays, where a different component clearly begins.

Because of the limited *ROSAT* bandpass and the sparse sampling at longer wavelengths in Figure 2, we can not entirely exclude a thermal origin for the optical-to-soft X-ray flux. Indeed, in 0405–123 the composite optical-to-UV spectrum shown by Corbin & Boroson (1996) appears steep with an upturn toward blue wavelengths, strongly suggestive of a blue bump. Also evidence for a thermal bump in the SED of 0923+392 is given by Elvis et al. (1994). Viewed from this perspective, the optical to soft X-ray emission of the four FSRQs of the present study could be thermal emission from an accretion disk. Indeed, thermal “bumps” at optical/UV have been observed for a few blazars, including 3C 345 and 3C 273 (Smith et al. 1986; von Montigny et al. 1997), and in 3C 279 during very low states (Pian et al. 1999). In 3C 273, the high-energy tail of the thermal component is detected with *ROSAT* and *SAX* (Leach, McHardy, & Papadakis 1995; Grandi et al. 1997), with slopes $\Gamma_{soft} \sim 2.4 - 2.8$, while a flat ($\Gamma_{hard} \sim 1.6$) continuum is measured at energies $\gtrsim 2$ keV (Grandi et al. 1997; Cappi et al. 1998; Haardt et al. 1998). The 0.2–2 keV component contributes $\sim 30\%$ to the total 0.2–10 keV flux, larger than in our targets (§ 3). The multiband continuum properties of 3C 273 are similar to our targets: from its contemporaneous SEDs compiled in Von Montigny et al. (1997), we derive K-corrected composite spectral indices $\alpha_{ro} = 0.61$, $\alpha_{ox} = 1.3$, and $\alpha_{rx} = 0.85$, well in the range of values observed for our four FSRQs (Table 1).

In the alternate hypothesis that the emission in the optical to soft X-ray bands has a non-thermal origin, the most plausible candidate is the high-energy tail of the synchrotron emission responsible for the longer wavelengths. These objects would thus be similar to the “intermediate” LBLs 0235+164 and 0716+714, which have similarly steep *ROSAT* spectra and flat X-ray continua at harder energies (Urry et al. 1996; Madejski et al. 1996; Cappi et al. 1994; Kubo et al. 1998) and synchrotron peaks at higher energies than in most LBLs. The extension of the synchrotron component to soft X-rays in 0405–123, 0923+392, and 1150+497 (Figure 2) would indicate unusually high electron energies and/or magnetic fields than in most FSRQs, making these objects outliers of the general blazar trend outlined above (§ 1).

¹No correction for the host galaxy emission was attempted; however, these sources are all distant enough that the galaxy contribution in the optical band is negligible.

The luminosities observed at the synchrotron peaks for our four FSRQs are consistent with those measured for the two intermediate LBLs mentioned above, 0235+164 and 0716+714 (Sambruna et al. 1996). However, the quasars have more luminous MgII emission lines by a factor $\gtrsim 10$ than the two LBLs. From Table 1, $L_{MgII} \sim (4 - 40) \times 10^{43}$ ergs s^{-1} for the three quasars where the MgII line was observed (0405–123, 0736+017, and 1150+497); for the intermediate LBLs, $L_{MgII} \lesssim 4 \times 10^{42}$ ergs s^{-1} is measured for 0235+164 (Cohen et al. 1987), while 0716+714 exhibits a featureless optical spectrum (Stickel, Fried, & Kühr 1993). This is in contrast with the unified paradigm of Ghisellini et al. (1998), where the coexistence of sources with similar peak frequencies and luminosities and largely ($\gtrsim 10$) different broad line luminosities is unexpected (e.g., their Figure 3).

In conclusion, our new *ASCA* observations of four FSRQs with steep soft X-ray spectra are consistent with a flat continuum similar to those of γ -ray-loud FSRQs, quite likely the onset of the Compton component. The *ASCA* slopes are significantly flatter than the *ROSAT* ones indicating a strong soft excess at low energies in 3/4 sources. A possible origin for the latter is thermal emission from an accretion disk (as in 3C 273 and 3C 445), and is supported in at least two cases (0405–123 and 0923+392) by independent longer-wavelength observations. Alternatively, the soft X-rays are the high-energy tail of the synchrotron emission responsible for the lower energies; in this case, their over-luminous emission lines would present a challenge for current unification schemes (Ghisellini et al. 1998). In either case, these sources qualify as highly unusual in the blazar class; further broad-band observations, especially in the critical optical-to-soft X-ray region, are needed to determine the origin of the soft excess and the role of these sources in the blazar class.

We acknowledge support from NASA contract NAS–38252 (RMS) and NASA grant NAG5–2538 (CMU). An anonymous referee provided constructive criticism which helped improving the paper. This research made use of the *ASCA* data archive at HEASARC, Goddard Space Flight Center, and of the NASA/IPAC Extragalactic Database (NED) which is operated by the Jet Propulsion Laboratory, California Institute of Technology, under contract with the National Aeronautics and Space Administration.

5. Appendix: Fits to the SIS data

It is well known that systematic effects are present in the two SIS detectors below 1–2 keV which lead to an overestimation of the column density (Dotani et al. 1996) by at least 3×10^{20} cm^{-2} . The latter has been increasing with the aging of the mission. A detailed study is under way (Yaqoob et al. 2000). In order to help quantifying the magnitude of

the effect, we performed spectral fits to the SIS0 and SIS1 data of our sources, which were taken in 1998 August–November (Table 2).

The SIS0 and SIS1 spectra were fitted separately with an absorbed power law, leaving the N_H free to vary. The results are reported in Table 5. Note that no excess absorption was detected with the *ROSAT* PSPC in any of the sources (Sambruna 1997). Comparing the fitted N_H from Table 5 to the value derived from the (non-simultaneous) *ROSAT* observations, we find that the column density measured with *ASCA* is always larger than the column measured with the PSPC by $\Delta N_H \sim 6 - 12 \times 10^{20} \text{ cm}^{-2}$ for SIS0 and $\Delta N_H \sim 6 - 18 \times 10^{20} \text{ cm}^{-2}$ for SIS1.

REFERENCES

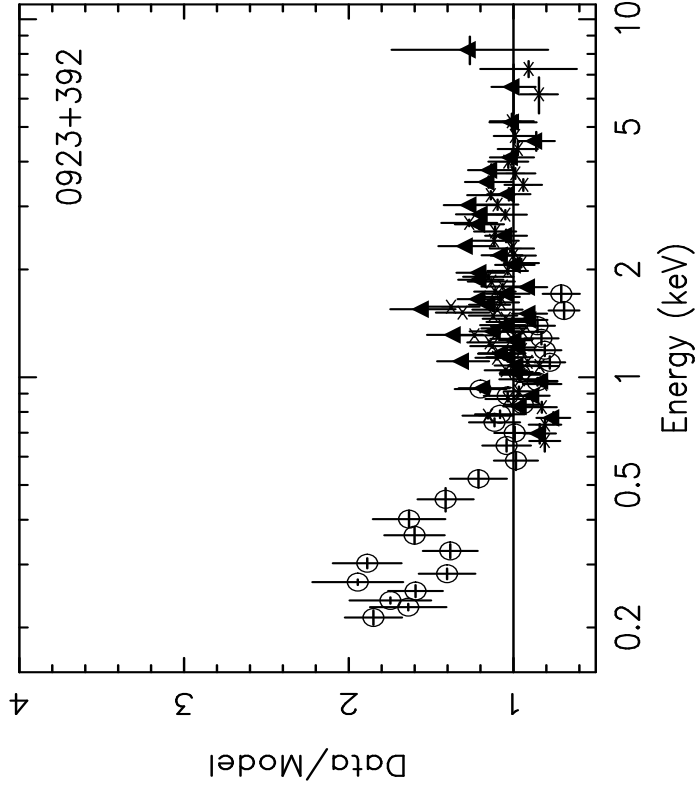
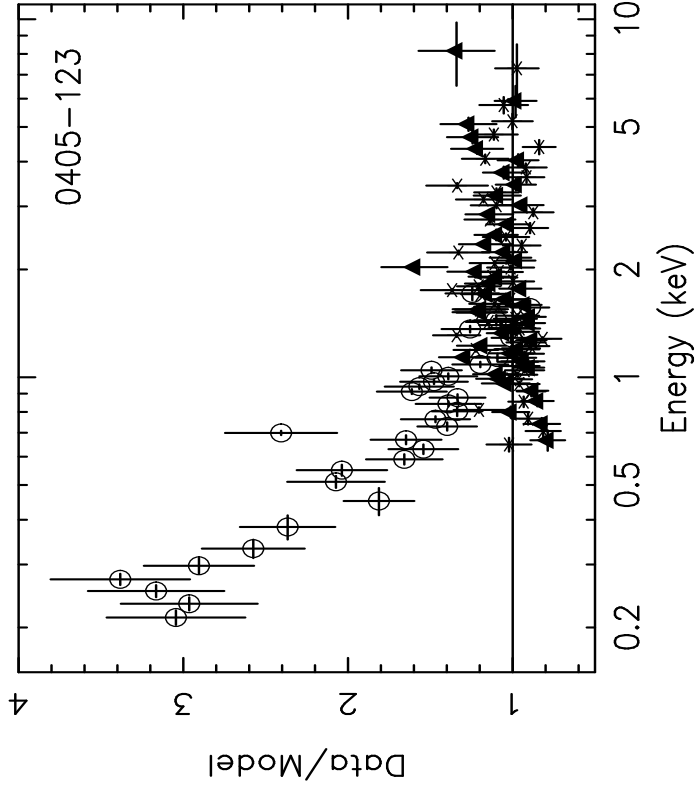
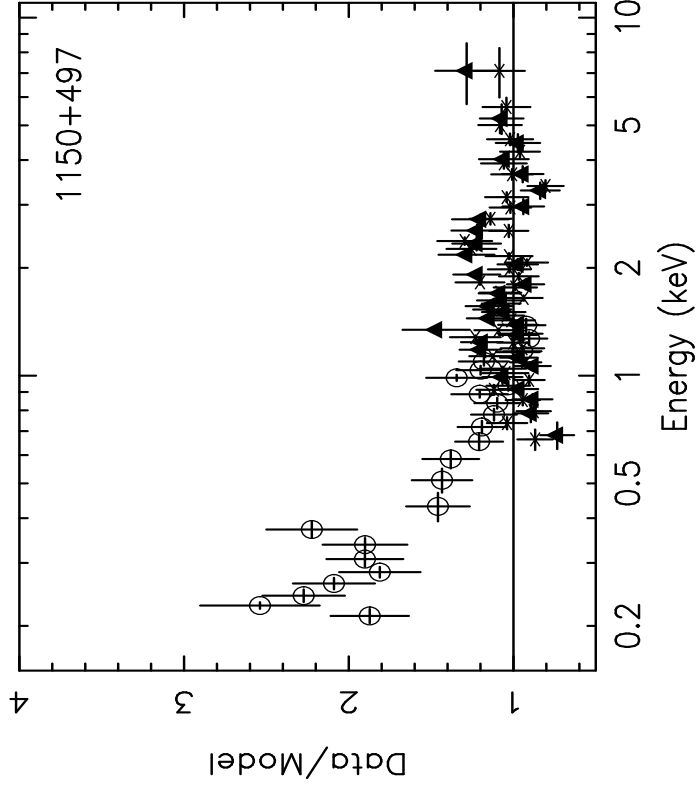
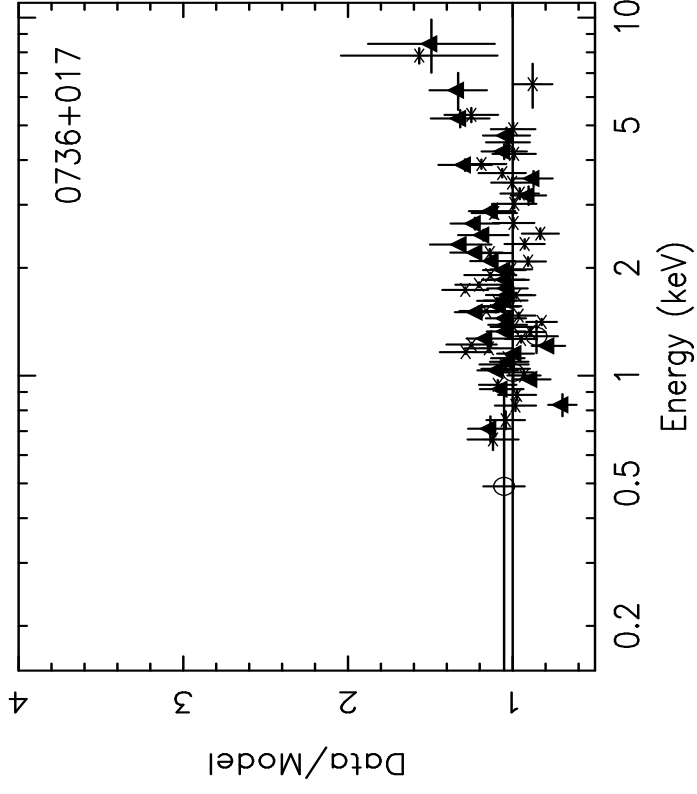
- Angel, J. R., & Stockman, H.S. 1980, *ARA&A*, 18, 321
- Blandford, R. D., & Rees, M. J. 1978, in Pittsburgh Conference on BL Lac Objects, Ed. A.M.Wolfe, Univ. of Pittsburgh Press, p. 328
- Cappi, M., Matsuoka, M., Otani, C., & Leighly, K. M. 1998, *PASP*, 50, 213
- Cappi, M., Comastri, A., Molendi, S., Palumbo, G. G. C., Della Ceca, R., & Maccacaro, T. 1994, *MNRAS*, 271, 438
- Carballo, R., Sanchez, S. F., Gonzalez-Serrano, J. I., Benn, C.R., & Vigotti, M. 1998, *AJ*, 115, 1234C
- Cohen, R. D., Smith, H. E., Junkkarineu, V. T., & Burbidge, E. M. 1987, *ApJ*, 318, 577
- Condon, J. J., Jauncey, D. L., & Wright, A. E. 1978, *AJ*, 83, 1036C
- Corbin, M. R. & Boroson, T. A. 1996, *ApJS*, 107, 69
- Dermer, C. D., Schlickeiser, R., & Mastichiasdis, A. 1992, *A&A*, 256, L27
- Dotani, T. et al. 1996, *ASCA News No.* 4, 3
- Elvis, M. et al. 1994, *ApJS*, 95, 1
- Elvis, M., Lockman, F.J., & Wilkes, B.J. 1989, *AJ*, 97, 777
- Fossati, G., Maraschi, L., Celotti, A., Comastri, A., & Ghisellini, G. 1998, *MNRAS*, 299, 433
- Fossati, G., Celotti, A., Ghisellini, G., & Maraschi, L. 1997, *MNRAS*, 289, 136
- Geldzahler, B. J., & Witzel, A. 1981, *AJ*, 86, 1306G
- Genzel, R., Pauliny-Toth, I. I. K., Preuss, E., & Witzel, A. 1976, *AJ*, 81, 1084G

- Ghisellini, G., Celotti, A., Fossati, G., Maraschi, L., & Comastri, A. 1998, MNRAS, 301, 451
- Ghisellini, G. & Madau, P. 1996, MNRAS, 280, 67
- Giommi, P., Ansari, S. G., & Micol, A. 1995, A&AS, 109, 267
- Grandi, P. et al. 1997, A&A, 325, L17
- Haardt, F. et al. 1998, A&A, 340, 35
- Hartman, R. C. et al. 1999, ApJS, 123, 79
- Hewitt, A. & Burbidge, G. 1989, ApJS, 69, 1
- Hyland A. R., & Allen D. A. 1982, MNRAS, 199, 943H
- Impey, C. D., & Neugebauer, G. 1988, 95, 307
- Kubo, H., Takahashi, T., Madejski, G., Tashiro, M., Makino, F., Inoue, S., & Takahara, F. 1998, ApJ, 504, 693
- Kühr, H., Witzel, A., Pauliny-Toth, I. I. K., & Nauber, U. 1981, A&AS, 45, 367
- Laurent-Muehleisen, S., Kollgaard, R. I., Ciardullo, R., Feigelson, E. D., Brinkmann, W., & Siebert, J. 1998, ApJS, 118, 127
- Leach, C. M., McHardy, I. M., & Papadakis, I. E. 1995, MNRAS, 272, 221
- Madejski, G., Takahashi, T., Tashiro, M., Kubo, H., Hartman, R., Kallman, T., & Sikora, M. 1996, ApJ, 459, 156
- Mannheim, K., & Biermann, P. L. 1992, A&A, 235, 21
- Maraschi, L., Ghisellini, G., & Celotti, A. 1992, ApJ, 397, L5
- Morrison, R. & McCammon, D. 1983, ApJ, 270, 119
- Nandra, K., George, I.M., Mushotzky, R.F., Turner, T.J., & Yaqoob, T. 1997, ApJ, 488, L91
- Owen, F. N., Porcas, R. W., Mufson, S. L., & Moffett, T. J. 1978, AJ, 83, 685O
- Owen, F. N., Porcas, R. W., & Neff, S. G. 1978, AJ, 83, 1009O
- Owen, F. N., Spangler, S. R., & Cotton, W. D. 1980, AJ, 85, 351O
- Padovani, P. 1992, MNRAS, 257, 404
- Padovani, P., Giommi, P., & Fiore, F. 1997, MNRAS, 284, 569
- Patnaik, A. R., Browne, I. W. A., Wilkinson, P. N., & Wrobel, J. M. 1992, MNRAS, 254, 655P

- Perlman, E. S., Padovani, P., Giommi, P., Sambruna, R. M., Jones, L. R., Tzioumis, A., & Reynolds, J. 1998, *AJ*, 115, 1253
- Pian, et al. 1999, *ApJ*, 521, 112
- Protheroe, R. J., & Biermann, P. L. 1997, *Aph*, 6, 293
- Sambruna, R. M., Eracleous, M., & Mushotzky, R. F. 1999, *ApJ*, 526, 60
- Sambruna, R. M., Ghisellini, G., Hooper, E., Kollgaard, R. I., Pesce, J. E., & Urry, C. M. 1999, *ApJ*, 515, 140
- Sambruna, R. M., Maraschi, L., & Urry, C. M. 1996, *ApJ*, 463, 444
- Sambruna, R. M. 1997, *ApJ*, 487, 536
- Scarpa, R., & Falomo, R. 1997, *A&A*, 325, 109
- Shimmins, A. J., & Wall, J. V. 1973, *AuJPh*, 26, 93S
- Sikora, M., Begelman, M. C., & Rees, M. J. 1994, *ApJ*, 421, 153
- Smith, P. S., Balonek, T. J., Heckert, P. A., & Elston, R. 1986, *ApJ*, 305, 484
- Stark, A.A., Gammie, C.F., Wilson, R.W., Bally, J., Linke, R.A., Heiles, C., & Hurwitz, M. 1992, *ApJS*, 79, 77
- Stickel, M., Fried, J. W., & Kühr, H. 1993, *A&AS*, 98, 393
- Tanaka, Y., Inoue, H., & Holt, S.S. 1994, *PASJ*, 46, L37
- Ulrich, M., Maraschi, L., & Urry, C. M. 1997, *ARA&A*, 35, 4454
- Urry, C. M. 1999, *Astroparticle Physics*, 11, 159
- Urry, C. M., et al. 1996, *ApJ*, 463, 424
- Urry, C. M. & Padovani, P. 1995, *PASP*, 107, 803
- von Montigny, C. et al. 1997, *ApJ*, 483, 161
- von Montigny, C. et al. 1995, *ApJ*, 440, 525
- Wall, J. V., Wright, A. E., & Bolton, J. G. 1976, *AuJPA*, 39, 1W
- Witzel, A., Pauliny-Toth, I. I. K., Geldzahler, B. J., & Kellermann, K. I. 1978, *AJ*, 83, 475W
- Wright, S. C., Mchardy, I. M., Abraham, R. G. 1998, *MNRAS*, 295, 799W
- Wright, A. & Otrupcek, R. 1990, *PKS90.C*, 0000W
- Yaqoob, T. et al. 2000, in prep.

Figure Captions

- Figure 1: Residuals of the fits to the *ASCA* data of the four FSRQs with a single power law plus Galactic absorption. The fits were performed jointly to all the four *ASCA* detectors, but only the SIS data are shown here for clarity (SIS0, *asterisks*; SIS1, *filled triangles*). The best-fit model is extrapolated into the *ROSAT* band and the non-simultaneous *ROSAT* data are plotted for comparison (*open circles*). A strong soft excess is apparent in 0405–123, 0923+392, and 1150+497, while the *ROSAT* spectrum of 0736+017 is consistent with the *ASCA* extrapolation.
- Figure 2: Spectral energy distributions (SEDs) of the four FSRQs using the *ASCA* data and non-simultaneous literature fluxes at longer wavelengths. The SEDs are characterized by large emission in the optical connecting smoothly to the soft X-rays. Both a thermal (from the accretion disk) and non-thermal (synchrotron emission from the jet) origin plausibly account for the optical to soft X-ray emission. Note the upturn at hard X-rays, marking the onset of the Compton component. *References:* For the radio data: Geldzahler & Witzel (1981), Kühr et al. (1981), Shimmins & Wall (1973), Wright and Otrupcek (1990), Condon, Jauncey, & Wright (1978), Wall, Wright, & Bolton (1976), Wills (1975), Owen, Spangler, & Cotton (1980), O’Dell et al. (1978), Owen et al. (1978), Owen et al. (1980), Witzel et al. (1978), Owen, Porcas, & Neff (1978), Genzel et al. (1976), Patnaik et al. (1992). For the IRAS data: Impey & Neugebauer (1988). For the IR and optical data: Hyland & Allen (1982), Carballo et al. (1998), Wright, Mchardy, & Abraham (1998). The *ROSAT* data were taken from Sambruna (1997) and the *ASCA* data are from this work.



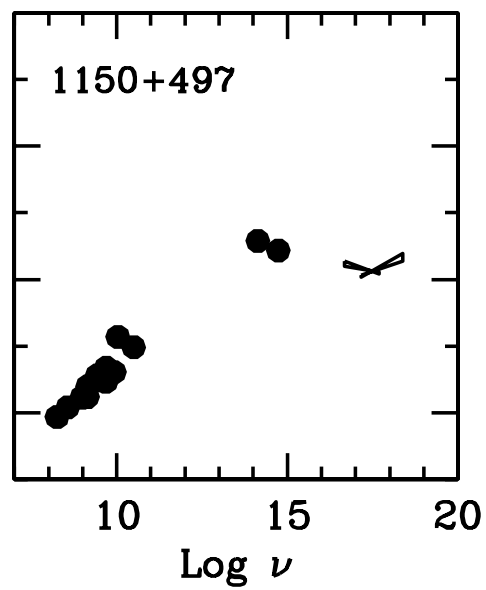
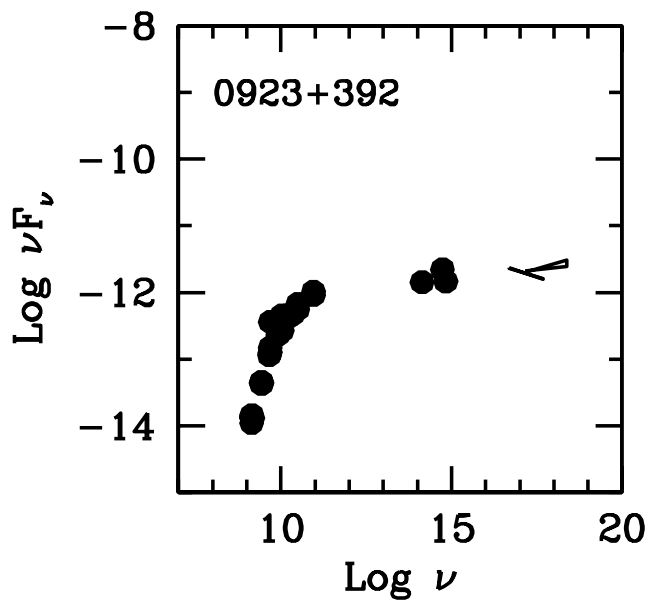
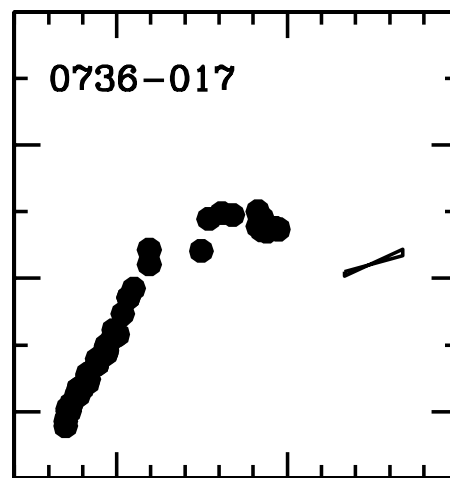
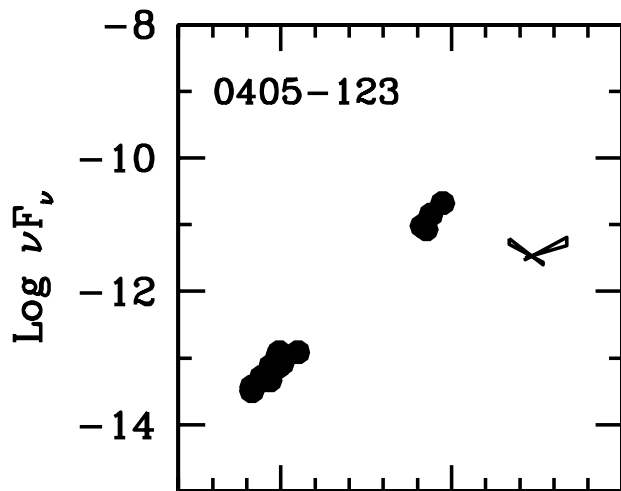


Table 1: Sample of “Steep-X-ray spectrum” FSRQs

Source	z	F_{radio}/V^a (Jy/mag)	Gal. N_H (10^{20} cm^{-2})	$\Gamma_{0.2-2.4 \text{ keV}}^b$	$F_{1 \text{ keV}}^b$ (μJy)	EW_{rest}^c (\AA)	$\text{Log } L_{BLR}^c$ (erg s^{-1})	α_{ro}^d	α_{ox}^d	α_{rx}^d
0405-123	0.574	2.05/14.8	3.7	2.33 ± 0.06	1.16 ± 0.05	35	44.6	0.51	1.31	0.78
0736+017	0.191	2.12/16.5	15.0	2.45 ± 0.30	0.57 ± 0.05	116	43.6	0.66	1.20	0.84
0923+392	0.698	8.73/17.9	1.6	$2.15-2.17^e$	$0.52-0.68^e$	38	44.1	0.82	0.96	0.87
1150+497	0.334	1.12/17.1	4.5	2.14 ± 0.05	0.55 ± 0.03	89	42.9	0.65	1.11	0.81

Notes: a=Observed radio (5 GHz) flux density and V magnitude (from Kühr et al. 1981 and Hewitt & Burbidge 1989, respectively); b=Photon index and 1 keV flux density from *ROSAT* PSPC (Sambruna 1997); c=Rest-frame equivalent width (EW) and luminosity (L_{BLR}) of the broad emission line of MgII except for 1150+497 ($H\beta$); d=Radio-to-optical, optical-to-X-ray, and radio-to-X-ray spectral indices, defined between 5 GHz, 5500 \AA , and 1 keV (from K-corrected fluxes, see text); e=Range of values from multiple *ROSAT* pointings.

Table 2: *ASCA* observations

Object	Date	Exposure ^a	SIS0 ^b	GIS2 ^b
	(UT)	(s)	(cts s ⁻¹)	(cts s ⁻¹)
0405-123	1998 Aug 9	26438	0.115 ± 0.002	0.092 ± 0.002
0736+017	1998 Oct 25	34090	0.090 ± 0.002	0.063 ± 0.002
0923+392	1998 Nov 01	30407	0.118 ± 0.002	0.085 ± 0.002
1150+497	1998 Nov 29	34212	0.096 ± 0.002	0.070 ± 0.002

Notes: a=Net exposure after data screening; b=Net count rates in 0.6–10 keV (SIS) and 0.7–10 keV (GIS).

Table 3: Spectral Fits to the ASCA Data: Absorbed Power Law

Object	N_H^a (10^{20} cm^{-2})	Γ^b	χ_r^2/dofs	$F_{2-10 \text{ keV}}^c$ ($10^{-12} \text{ ergs cm}^{-2} \text{ s}^{-1}$)
0405-123	3.74 (fix)	1.69 ± 0.03	0.97/420	5.4
	$10.08^{+2.11}_{-3.52}$	$1.79^{+0.04}_{-0.06}$	0.95/419	
0736+017	1.5 (fix)	1.76 ± 0.04	1.07/419	3.6
	$16.0^{+4.1}_{-2.7}$	$1.78^{+0.07}_{-0.05}$	1.07/418	
0923+392	1.6 (fix)	1.73 ± 0.02	1.11/441	
	$10.8^{+3.7}_{-2.4}$	$1.88^{+0.07}_{-0.03}$	1.03/440	4.1
1150+497	2.1 (fix)	1.66 ± 0.04	0.89/402	3.5
	$8.2^{+2.8}_{-3.2}$	$1.77^{+0.05}_{-0.06}$	0.87/401	

Notes: a=Column density in the direction to the source. When fixed (fix), the column was held to the Galactic value during the fit (from Table 1); b=Photon index; c=Observed flux in 2–10 keV.

Table 4: Spectral Fits to the *ROSAT* + *ASCA* Data

Object	Double Power Law ^a			Bremsstrahlung + P.Law ^a			Blackbody + P.Law ^a			(10)
	Γ_1	Γ_2	χ_r^2/dofs	kT (keV)	Γ	χ_r^2/dofs	kT (keV)	Γ	χ_r^2/dofs	
0405-123	$2.81^{+0.61}_{-0.23}$	$1.55^{+0.18}_{-0.17}$	0.95/498	0.23 ± 0.04	1.76 ± 0.04	0.93/498	0.083 ± 0.008	1.79 ± 0.04	0.94/498	
0736+017	1.81 ± 0.05	...	1.04/426	
0923+392	$3.0^{+1.0}_{-0.2}$	$1.80^{+0.08}_{-0.19}$	0.99/501	$0.20^{+0.07}_{-0.09}$	1.84 ± 0.04	0.99/502	$0.08^{+0.01}_{-0.02}$	1.85 ± 0.04	0.99/502	
1150+497	$3.98^{+0.52}_{-0.33}$	$1.68^{+0.08}_{-0.09}$	0.84/456	$0.13^{+0.02}_{-0.04}$	1.79 ± 0.05	0.87/456	$0.057^{+0.007}_{-0.011}$	1.79 ± 0.05	0.87/456	

Notes: a=During the fits, the column density was fixed to the Galactic values (from Table 1), except for the SIS0 and SIS1 data where it was left free to vary (because of the calibration uncertainties at lower energies of the latter two detectors; see § 2.2).

Table 5: Fits to the SIS data

Object	SIS0			SIS1		
	N_H (10^{20} cm^{-2})	Γ	χ_r^2/dofs	N_H (10^{20} cm^{-2})	Γ	χ_r^2/dofs
0405-123	$9.9^{+4.4}_{-4.0}$	1.79 ± 0.09	0.89/98	8.7 ± 4.6	1.70 ± 0.09	0.89/91
0736+017	$14.4^{+5.1}_{-4.7}$	1.77 ± 0.11	0.94/91	$20.5^{+6.9}_{-6.1}$	$1.74^{+0.14}_{-0.12}$	1.4/80
0923+392	$13.6^{+4.5}_{-3.9}$	1.94 ± 0.10	0.75/91	$11.8^{+5.2}_{-4.9}$	1.86 ± 0.11	1.04/84
1150+497	$6.9^{+4.1}_{-5.0}$	1.74 ± 0.11	0.67/89	$12.3^{+6.2}_{-5.4}$	1.81 ± 0.14	0.93/75